

Assessment of Liver Viscoelasticity Using Multifrequency MR Elastography

Patrick Asbach,¹ Dieter Klatt,¹ Uwe Hamhaber,² Jürgen Braun,² Rajan Somasundaram,³ Bernd Hamm,¹ and Ingolf Sack^{1*}

MR elastography (MRE) allows the noninvasive assessment of the viscoelastic properties of human organs based on the organ response to oscillatory shear stress. Shear waves of a given frequency are mechanically introduced and the propagation is imaged by applying motion-sensitive gradients. An experiment was set up that introduces multifrequency shear waves combined with broadband motion sensitization to extend the dynamic range of MRE from one given frequency to, in this study, four different frequencies. With this approach, multiple wave images corresponding to the four driving frequencies are simultaneously acquired and can be evaluated with regard to the dispersion of the complex modulus over the respective frequency. A viscoelastic model based on two shear moduli and one viscosity parameter was used to reproduce the experimental wave speed and wave damping dispersion. The technique was applied in eight healthy volunteers and eight patients with biopsy-proven high-grade liver fibrosis (grade 3–4). Fibrotic liver had a significantly higher ($P < 0.01$) viscosity ($14.4 \pm 6.6 \text{ Pa} \cdot \text{s}$) and elastic moduli ($2.91 \pm 0.84 \text{ kPa}$; $4.83 \pm 1.77 \text{ kPa}$) than the viscosity ($7.3 \pm 2.3 \text{ Pa} \cdot \text{s}$) and elastic moduli ($1.16 \pm 0.28 \text{ kPa}$; $1.97 \pm 0.30 \text{ kPa}$) of normal volunteers. Multifrequency MRE is well suited for the noninvasive differentiation of normal and fibrotic liver as it allows the measurement of rheologic material properties. *Magn Reson Med* 60:373–379, 2008. © 2008 Wiley-Liss, Inc.

Key words: magnetic resonance elastography; wave speed dispersion; viscoelasticity; liver; cirrhosis; fibrosis; multifrequency MRE

Diffuse liver disease can be diagnosed by morphologic criteria such as size, contour, and shape of the liver. However, these findings occur late in the course of the disease, usually at a point when it has reached an irreversible stage (1–3). During a patient's clinical workup, an alteration of the size and stiffness of the liver can be subjectively detected by manual palpation.

Based on ultrasound or MR imaging a more objective approach can be selected to characterize the mechanical properties of tissues by means of elastography (4–7). In MRI, motion encoding enables the visualization of tissue-constitutive parameters by imaging harmonic shear waves

propagating in organs (6). In transient ultrasound elastography, the velocity of a shock-wave impulse through liver tissue is measured for grading the stage of fibrosis (8,9). MR elastography (MRE) has recently been shown to enable the detection of liver fibrosis by using a monofrequency approach by which shear waves of one specific frequency are introduced into the liver and elastic and viscous moduli can be calculated from the respective wave images (10–13).

As demonstrated by several researchers (14–17), the wave propagation speed and the damping of shear waves in soft tissue increases with increasing harmonic driving frequency due to the dispersion of elastic waves in viscous media. Here, the dispersion of shear waves is exploited for the viscoelastic characterization of normal and fibrotic liver. Therefore, superposed tissue oscillations at multiple harmonic driving frequencies are acquired in a single MRE scan using broad-band frequency encoding (15,18–20). In the following the technical details of multifrequency MRE on human liver are introduced and appropriate data evaluation is developed. The protocol is applied in healthy volunteers and patients based on the hypothesis that normal and fibrotic liver tissue can be differentiated with high specificity and sensitivity by their elastodynamic behavior.

THEORY

In multifrequency MRE the broadband motion-encoding characteristics of a sinusoidal gradient is essential for the accumulation of a spin phase ϕ caused by harmonic vibrations at different frequencies. The efficiency ε of encoding a specific frequency component f by a sinusoidal motion encoding gradient (MEG) is the ratio between the measured phase amplitude ϕ in the images and the physical displacement amplitude u in units of radians per micrometer (μm):

$$\varepsilon = \frac{\gamma g \tau \sin(\pi N \tau f)}{\pi(1 - \tau^2 f^2)}. \quad [1]$$

where g , τ and N denote amplitude, duration, and number of sinusoidal MEG periods, respectively; γ is the gyromagnetic ratio. Equation [1] is deduced from Ref. 20 with the extension of arbitrary N . By limiting the attention to two-dimensional (2D) wave images acquired with through-plane motion sensitization, u is henceforth given as a scalar wave field $u(x,y,t)$. A plane wave approach yields for $u(x,y,t)$ in the Fourier domain

$$U(x,y,\omega) = U_0 \exp \left[i \omega \left(\frac{\mathbf{n} \cdot \mathbf{r}}{c} \right) - \Gamma \mathbf{n} \cdot \mathbf{r} \right], \quad [2]$$

¹Department of Radiology, Charité-Universitätsmedizin Berlin, Campus Mitte, Berlin, Germany.

²Institute of Medical Informatics, Charité-Universitätsmedizin Berlin, Campus Benjamin Franklin, Berlin, Germany.

³Department of Gastroenterology, Rheumatology and Infectiology, Charité-Universitätsmedizin Berlin, Campus Benjamin Franklin, Berlin, Germany.

Grant sponsor: German Research Foundation; Grant number: Sa/901-3.

*Correspondence to: Ingolf Sack, PhD, Department of Radiology, Charité-Universitätsmedizin Berlin, Charitéplatz 1, 10117 Berlin, Germany. E-mail: ingolf.sack@charite.de

Received 28 August 2007; revised 22 January 2008; accepted 28 February 2008.

DOI 10.1002/mrm.21636

Published online in Wiley InterScience (www.interscience.wiley.com).

© 2008 Wiley-Liss, Inc.

with the wave normal vector $\mathbf{n}(x,y)$, the position vector $\mathbf{r}(x,y)$, and the initial deflection at the source of the waves U_0 . Variables c , Γ , and ω denote wave speed, wave damping, and the angular driving frequency, respectively. Equation [2] solves the equation of motion of an isotropic material subjected to oscillatory shear stress:

$$\rho\omega^2U + G(\omega)\Delta U = 0; \quad \Delta = \left(\frac{\partial^2}{\partial x^2} + \frac{\partial^2}{\partial y^2} \right). \quad [3]$$

$G(\omega)$ and ρ represent the complex shear modulus and the density of the material. Solving Eq. [3] for G yields:

$$G(\omega) = - \frac{\rho\omega^2U}{\Delta U}. \quad [4]$$

In the plane wave model, wave speed and damping are related to the complex modulus by:

$$c(\omega) = \frac{1}{\Re \left[\sqrt{\frac{\rho}{G(\omega)}} \right]} \text{ and } \Gamma(\omega) = \omega \Im \left[\sqrt{\frac{\rho}{G(\omega)}} \right], \quad [5]$$

with \Re and \Im as symbols for the real and the imaginary part of a complex number, respectively. In the theory of viscoelasticity, the rheological properties of the material are modeled by a complex modulus $G_M(\omega)$ derived from a specific combination of parallel and serial spring and dashpot elements. Here, the model for a standard linear solid (SLS) is used, which incorporates three viscoelastic modeling parameters:

$$G_M(\omega) = \frac{\mu_1\mu_2 + i\omega\eta(\mu_1 + \mu_2)}{\mu_2 + i\omega\eta}, \quad [6]$$

where η and μ_2 refer to the viscosity and elasticity of a Maxwell body, i.e., serial dashpot and spring elements, respectively. Variable μ_1 is related to the elasticity of a spring element that is parallel to the Maxwell elements. Inserting the model $G_M(\omega)$ into Eq. [5] predicts the increase of wave speed and wave damping with increasing driving frequency. Within the limit of static deformation ($\omega = 0$), c is given by $\sqrt{\mu_1/\rho}$ and Γ equals 0, while at high frequencies c and Γ approach $\sqrt{(\mu_1 + \mu_2)/\rho}$ and $\mu_2^2/2\eta\sqrt{\rho/(\mu_1 + \mu_2)^3}$, respectively. For further reading on viscoelasticity, see Ref. 21.

MATERIALS AND METHODS

Volunteers and Patients

A total of eight healthy volunteers and eight patients with biopsy-proven liver fibrosis (grade 3–4) were examined using multifrequency MRE. Each subject was examined at least twice at different slice positions within one MRE study setup. An indication about reproducibility was gained by follow-up studies separated by days and performed by different operators. The numbers of MRE acquisitions and follow-up studies as well as the demographic data of each subject are given in Table 1. Institutional

Table 1
Liver Viscoelasticity According to the SLS-Model Found in Eight Volunteers and Eight Patients*

Case	Healthy volunteers				Patients			
	1	2	3	4	5	6	7	8
Symbol	▽	▽	○	◇	☆	□	△	▲
Studies	6/3	4/2	5/2	4/2	4/2	4/2	7/3	4/2
Age/sex	26/m	30/f	32/f	34/m	35/m	35/m	46/m	69/m
μ_1 (kPa)	1.5 (0.3)	1.8 (0.3)	1.2 (0.3)	0.9 (0.3)	1.1 (0.2)	1.0 (0.3)	1.2 (0.3)	2.8 (1.0)
$\mu_2 + \mu_1$ (kPa)	3.6 (0.5)	4.4 (0.9)	3.2 (0.4)	2.9 (0.7)	2.6 (0.3)	2.8 (0.4)	3.2 (0.4)	7.3 (1.9)
η (Pa s)	6.4 (1.7)	6.3 (0.7)	6.8 (2.9)	8.5 (2.2)	4.8 (1.3)	7.4 (3.5)	7.3 (3.5)	11.9 (2.0)
Δr	-3.0 (1.0)	-1.9 (1.4)	-3.7 (0.9)	-4.2 (2.2)	-5.0 (0.7)	-3.9 (1.5)	-3.3 (1.2)	0.5 (0.1)

*The symbols correspond to those in Figs. 5 and 6. The number of studies is given with both the total number of examinations and the number of follow-up studies on different days separated by a backslash. Tolerances of the viscoelastic parameters are given in brackets (\pm SD of individual results shown in Fig. 6). Δr indicates the quality of separation between healthy ($\Delta r < 0$) and diseased liver ($\Delta r > 0$).
m = male, f = female.

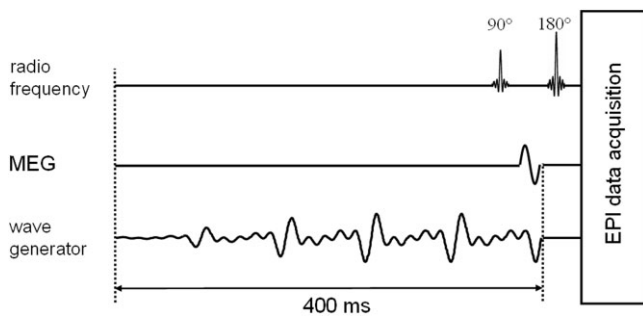


FIG. 1. Timing of MRE sequence and vibration generator output. The MEG shown is parallel to the slice gradient direction for capturing through-plane motions.

review board approval was obtained, and informed consent was obtained from all subjects.

MRI

All scans were performed on a 1.5-T MR scanner (Magnetom Sonata; Siemens Medical Solutions, Erlangen, Germany) using a 12-channel phased-array surface coil with six elements anterior and six elements posterior to the torso. A single-shot spin-echo echo-planar imaging (EPI) sequence with sinusoidal MEG ($g = 20 \text{ mT/m}$, $\tau = 20 \text{ ms}$, and $N = 1$) in the direction of slice selection was used to acquire axial phase contrast wave images with the following parameters: $TR = 500 \text{ ms}$, $TE = 64 \text{ ms}$, slice thickness = 10 mm , field of view = 300 mm , matrix size = 64×128 , acquisition time = 40 s , divided into two breathholds. A transistor-transistor logic (TTL)-triggered pulse was given from the sequence to the wave generator 400 ms ahead of the end of the MEG (Fig. 1). This delay was increased 40 times by an increment of 2 ms to achieve a frequency resolution of 12.5-Hz multiples. A reference

data set of monochromatic excitation was acquired in volunteer 5 using eight phase offsets at each frequency. To calculate phase-difference wave images, two phase images with inverse MEG amplitude were acquired at each time point.

Wave Generation

Patients and volunteers were examined in a supine position. Shear waves were introduced into the liver via a transducer positioned below the right costal arch. Oscillations were driven by a remote vibration generator (Fig. 2) with main deflection along the anterior-posterior direction. Four sinusoidal waveforms with frequencies of 25.0 , 37.5 , 50.0 , and 62.5 Hz were superposed with linearly increasing amplitude to minimize transient effects (Fig. 1). The relative amplitude of each waveform was doubled with each 12.5-Hz increment. Equation [1] was used prior to the experiments to simulate the encoding efficiency at the four driving frequencies used. A single-cycle MEG of 20-ms lengths was found as a tradeoff between encoding efficiency and TE. The efficiency of such MEG for encoding the vibration components is $\epsilon = 4.5, 5.5, 5.3,$ and $4.3 \times 10^4 \text{ rad/m}$ from 25.0 to 62.5 Hz , respectively.

Postprocessing

Time-resolved phase difference wave images were temporally Fourier transformed. The complex wave images $U(x,y,\omega)$ were taken at $25.0, 37.5, 50.0,$ and 62.5 Hz and filtered to remove compression wave components and noise by a spatial two-dimensional (2D) Butterworth filter with empirically-derived thresholds given by $a \cdot \exp(-bf) + c$, with $a = 0.017(1.137) \text{ m}$, $b = 0.054(0.058) \text{ sec}$, and $c = 0.01(0.051) \text{ m}$ for the lower (upper) cutoff wavelengths. $G(\omega)$ was then calculated according to Eq. [4], assuming a density of 1050 kg/m^3 and averaging the

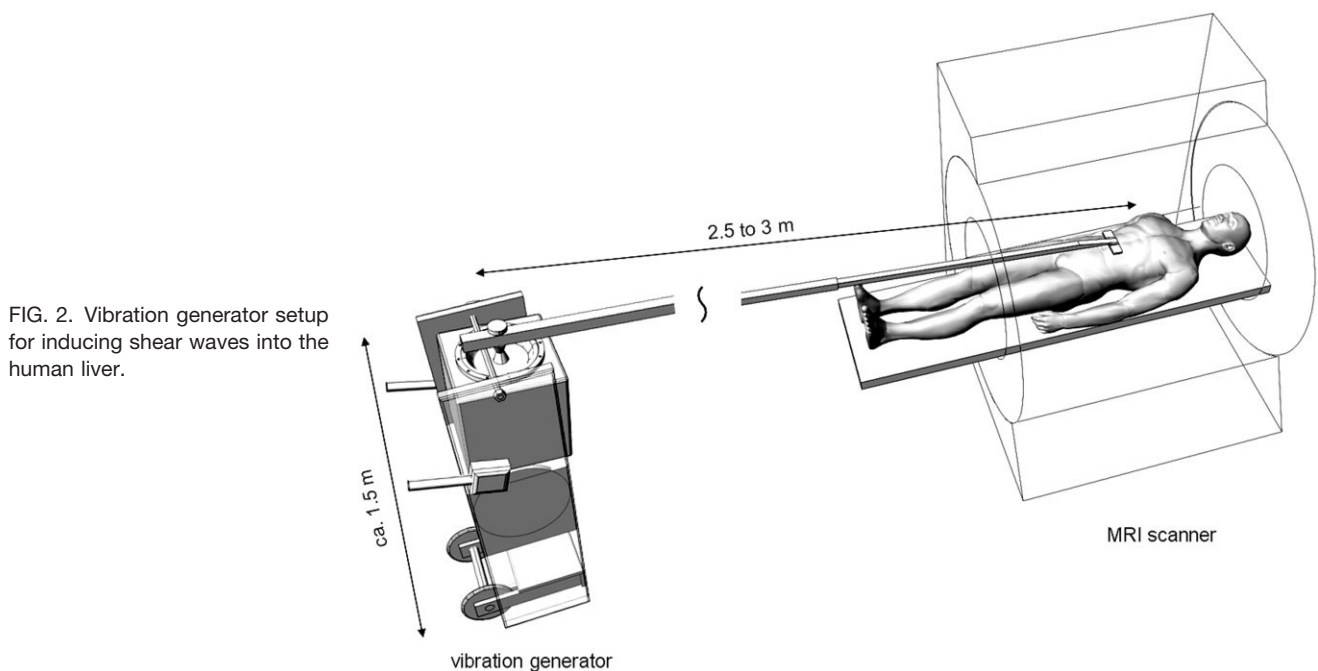


FIG. 2. Vibration generator setup for inducing shear waves into the human liver.

spatially-resolved modulus within a wave-energy-dependent region of interest (ROI) of the liver (12). The ROI was placed within the right hepatic lobe, covering the maximum possible cross-section of the right lobe, avoiding large vessels and areas with pulsation artifacts from vascular structures. $G(\omega)$ was used in Eq. [5] to derive $c(\omega)$ and $\Gamma(\omega)$. Numerical dispersion curves were fitted to the experimental $c(\omega)$ and $\Gamma(\omega)$ data by a least-square minimization using $G_M(\omega)$ of Eq. [6]. The resulting viscoelastic constants were taken as components of a vector (\mathbf{R}) in the parameter domain given by $\xi_1 = \mu_1/1$ kPa, $\xi_2 = (\mu_1 + \mu_2)/1$ kPa, and $\xi_3 = \eta/1$ Pa · s. To obtain the best separation between data of healthy and diseased liver, an ellipsoid, $(\lambda_1\xi_1)^2 + (\lambda_2\xi_2)^2 + (\lambda_3\xi_3)^2 = r^2$, was fitted into the parameter space by varying the λ coefficients. The success of separation was measured by means of the area under the receiver operating characteristic (ROC) curve (AUROC) of Δr , which is the Euclidean distance between \mathbf{R} and the point where the ray along \mathbf{R} crosses the ellipsoidal threshold surface.

RESULTS

Fibrotic liver revealed significantly higher ($P < 0.01$) viscosity η (14.4 ± 6.6 Pa · s) and elastic moduli ($\mu_1 = 2.91 \pm 0.84$ kPa; $\mu_2 = 4.83 \pm 1.77$ kPa) than the viscosity η (7.3 ± 2.3 Pa · s) and elastic moduli ($\mu_1 = 1.16 \pm 0.28$ kPa; $\mu_2 = 1.97 \pm 0.30$ kPa) of normal volunteers.

Figure 3 shows multifrequency MRE images of the normal liver of one volunteer decomposed into the four oscillation components. The scaling factor of the color bar reveals the decrease of the wave amplitude with increasing frequency. The phase-to-noise ratio of the wave images is determined by the efficiency of the MEG in encoding harmonic motions, which has its maximum at ~ 41 Hz driving frequency (Eq. [1]). The corresponding wave speed contrast images are shown in Fig. 4, indicating that wave speed increases with higher frequency.

Figure 5 demonstrates the fit of c and Γ dispersion data measured in volunteer 5 and patient 8 by the rheological model of Eq. [6]. Similar dispersion curves were obtained by repeating the wave data acquisition for each frequency component using monochromatic excitation (data shown for the volunteer). The different course of the curves in normal liver and fibrotic liver clarifies that the shear waves propagate slower and show stronger damping in healthy liver tissue. The fit curves corresponding to the SLS model reproduce well the experimentally found dispersion in both healthy and diseased liver. Viscoelastic parameters used for simulating the experiments are given in Table 1. There, the mean of the parameters and their standard deviations (SDs) from multiple studies of the same volunteer are listed. The results of all individual experiments are plotted in Fig. 6. A 3D viscoelastic parameter space is obtained due to the multidimensionality of the rheologic model used. The plotted ellipsoid corresponds to the coefficients $\lambda_1 = 5$, $\lambda_2 = 7$, and $\lambda_3 = 17$. These values yield a separation given by the sign of Δr in Table 1, i.e., the data were within ($\Delta r < 0$) or outside ($\Delta r > 0$) of the threshold surface. The high AUROC of 0.994 is due to the excellent separation with only one false-negative assignment (patient 3). The range of possible threshold values for μ_1 , $\mu_1 + \mu_2$, and η yielding the same AUROC are given in Fig. 7.

DISCUSSION

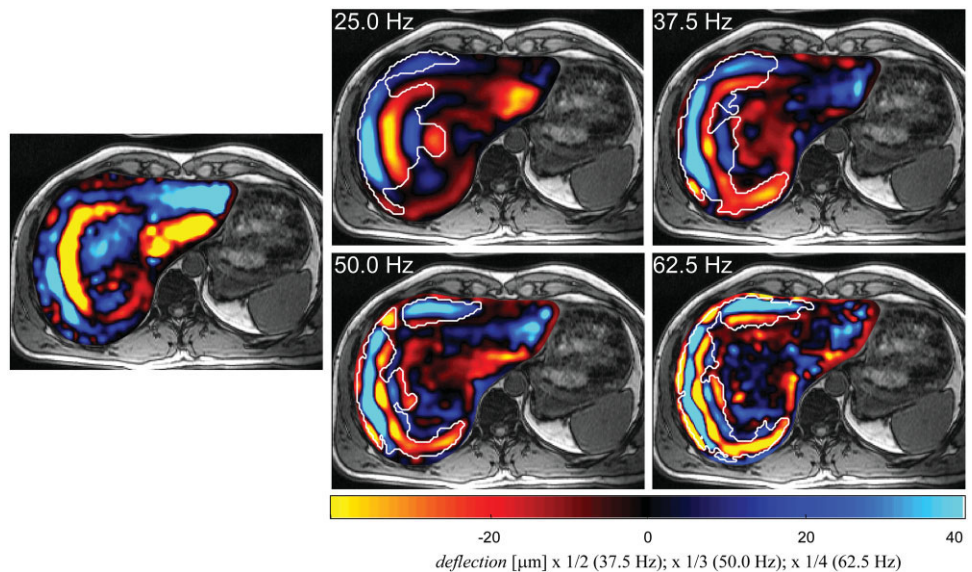
Multifrequency MRE allows the characterization of liver cirrhosis on an elastodynamic basis in a single time-resolved experiment. Our basic finding is that both healthy and diseased liver display a frequency-dependent elastodynamic behavior. This observation agrees with numerous studies on excised tissue specimens using oscillatory shear tests (14,22–24). Therefore, any specific viscoelastic parameter deduced by shear wave-based elastography has to be given in the context of the underlying viscoelastic model with notation of the explored frequency range. The method introduced is able to map the dispersion of the complex modulus at four frequencies, resulting in eight independent equations to be solved for three viscoelastic parameters. In a pretest with normal volunteers, each frequency component was determined separately using a monochromatic excitation and the data were compared to the superimposed multifrequency excitation. Similar dispersion curves in both experiments revealed that decomposing of each of the four oscillating frequency components in the multifrequency excitation is equal to a monochromatic excitation (see Fig. 5).

It is important to note that our current protocol is not time-optimized as only two phase offsets have to be acquired to resolve a single frequency component of a harmonic oscillation. Typically, four phase offsets are used in MRE of the liver (25). An optimized sampling of the four vibration components used could comprise 10 offsets with an increment of 8 ms, resulting in a four-fold acceleration of the data acquisition. However, using fast single-shot EPI-MRE, measurement time was not highly crucial in our experiments and the protocol was adjusted to match two breathholds. Within this limit a maximum of data was acquired to improve the SNR of the wave images. In any case, it is preferable to synchronously encode multifrequency vibrations instead of applying consecutive monofrequency MRE experiments with a variable driving frequency. The data shown demonstrate the high consistency and reproducibility of multifrequency MRE, which is hard to achieve by monochromatic wave excitation at different frequencies.

The evaluation of multifrequency data benefits from the stability of a least square fit of an overdetermined system of equations. This improves the accuracy of the results compared to a monofrequency assignment of $\mu \equiv \Re(G)$ and $\eta \equiv \Im(G)/\omega$ as done by the Voigt model. The three-parameter SLS model used here was chosen after comparing the outcome of several two-, three-, and four-parameter models, such as the Voigt, Maxwell, and Jeffreys model (a detailed study is given in Ref. 15). In this context, the rheological foundations of these model functions were given minor attention, since in clinical use the fit of elastodynamic data mainly focuses on grading liver fibrosis.

The wave speed dispersion and the wave damping dispersion significantly differed between normal volunteers and patients with liver fibrosis, which allowed a clear separation of the two groups. The different course of the two curves obviates that the shear waves propagate slower and show stronger damping in normal liver than in fibrotic liver. Moreover, the differences increase with higher frequencies. These findings are similar to those reported in

FIG. 3. Wave images, $\Re(U(x,y,f))$ superimposed to T_1 -weighted MRI scans as acquired by multifrequency MRE. The single image on the left-hand side shows a snapshot of the waves before decomposition into the vibration components shown on the right-hand side. The automatic ROI selection dependent on the magnitude wave amplitude ($|U(x,y,f)|$) is demarcated by white lines. Please note that the color scale has to be multiplied by different factors.



previous studies, since the elasticity and viscosity of high-grade liver fibrosis were in the same range, indicating that mono- and multifrequency experiments are comparable in this respect (10,11). Previous studies in animals and in humans have shown that it is possible to differentiate normal from fibrotic liver by MRE (10,11,13). However, larger patient populations with different stages of fibrosis are necessary to investigate the potential of MRE as a clear alternative to liver biopsy. The possibility of obtaining information such as wave speed dispersion and wave damping may further increase the accuracy of MRE to detect pathologic changes of organ texture. MRE may be particularly suited for following patients with known liver disease to avoid repeated biopsies. One patient examined at our institution (patient 3 in Table 1) had a diagnosis of grade III liver fibrosis established by biopsy 18 months

prior to MRI. Since then, the patient had improved clinically and was free of symptoms at the time of the MRE study. Both the liver enzymes and the laboratory values for inflammatory activity had normalized and the coagulation factors were also within the normal range. The viscoelastic parameters were almost normal, with $\mu_1 = 1.9 \pm 0.1$ kPa, $\mu_1 + \mu_2 = 4.3 \pm 0.1$ kPa, and $\eta = 5.9 \pm 0.1$ Pa · s. Because of this constellation, the decision was made to follow the patient without a repeated liver biopsy. The suggested threshold surface drawn in Fig. 6 was established to discriminate the subgroup of healthy volunteers (including patient 3) from the patient group. Also, any other implicit function in the parameter domain can be used if the threshold lies within both cohorts. It is therefore difficult to install fixed thresholds, since their values and tolerance limits depend on each other. An attempt was made in Fig. 7 to give a hint about the stability of the separation. Here, the range is graphically indicated; the viscoelastic parameters separate the groups of healthy volunteers and patients. More data are obviously needed to refine this plot.

One limitation of this feasibility study is the small number of eight patients and the fact that all patients had high-grade liver fibrosis. Thus the multifrequency MRE approach was not validated for low grades of liver fibrosis. The cutting edge of MRE will be the sensitivity to detect the different stages of liver fibrosis and especially the very early stages at which therapy can lead to a reversal of fibrogenesis. First results about grading the different stages of liver fibrosis have recently been presented and are very promising (25).

CONCLUSIONS

Accurate noninvasive disease assessment is more welcome than any other type of invasive testing in terms of patient acceptance, clinical work flow, and, ultimately, cost. This also applies to diagnosing liver fibrosis. Since all investigated viscoelastic parameters show a significant difference between normal and cirrhotic liver, multifrequency MRE seems to enable a differentiation between

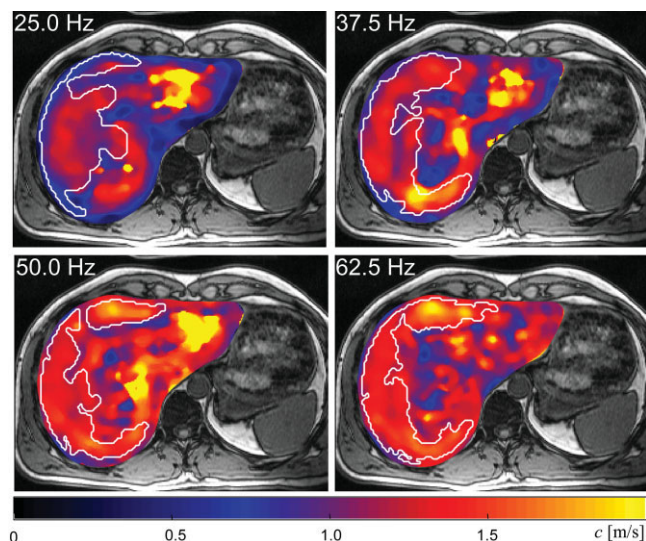


FIG. 4. Shear wave speed images derived after wave inversion using Eq. [5]. The white demarcations correspond to the ROIs shown in Fig. 3.

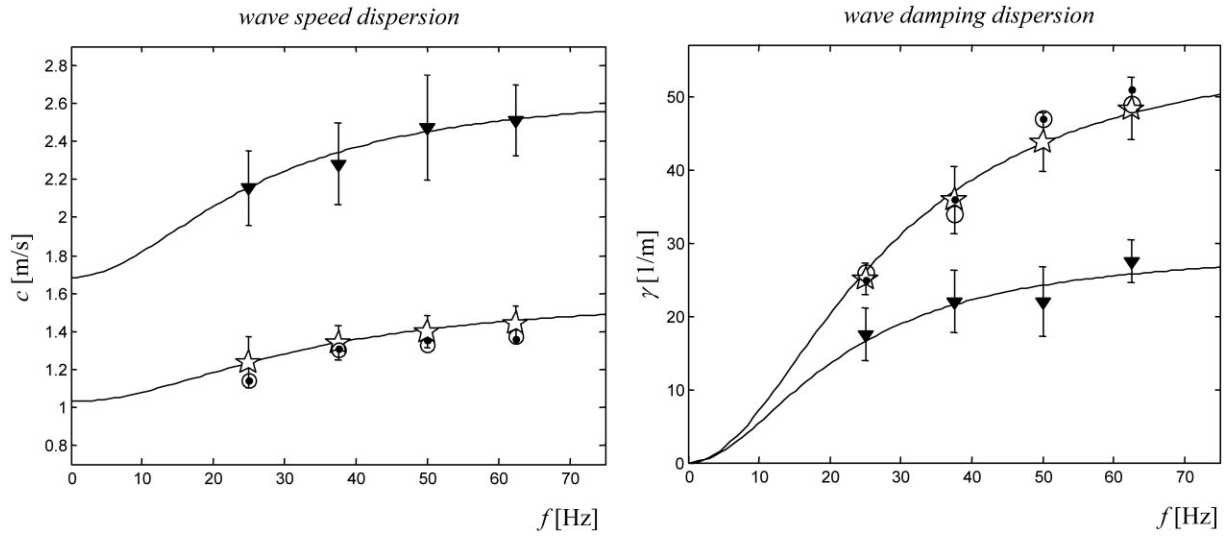


FIG. 5. Experimental (symbols) and simulated (line graphs) wave speed and wave damping dispersion relations found in volunteer 5 (☆) and patient 8 (▼). Conventional monofrequency MRE studies at four frequencies are shown for the healthy volunteer (●) superimposed to a corresponding multifrequency study (○). Error bars indicate ± SD of independent studies.

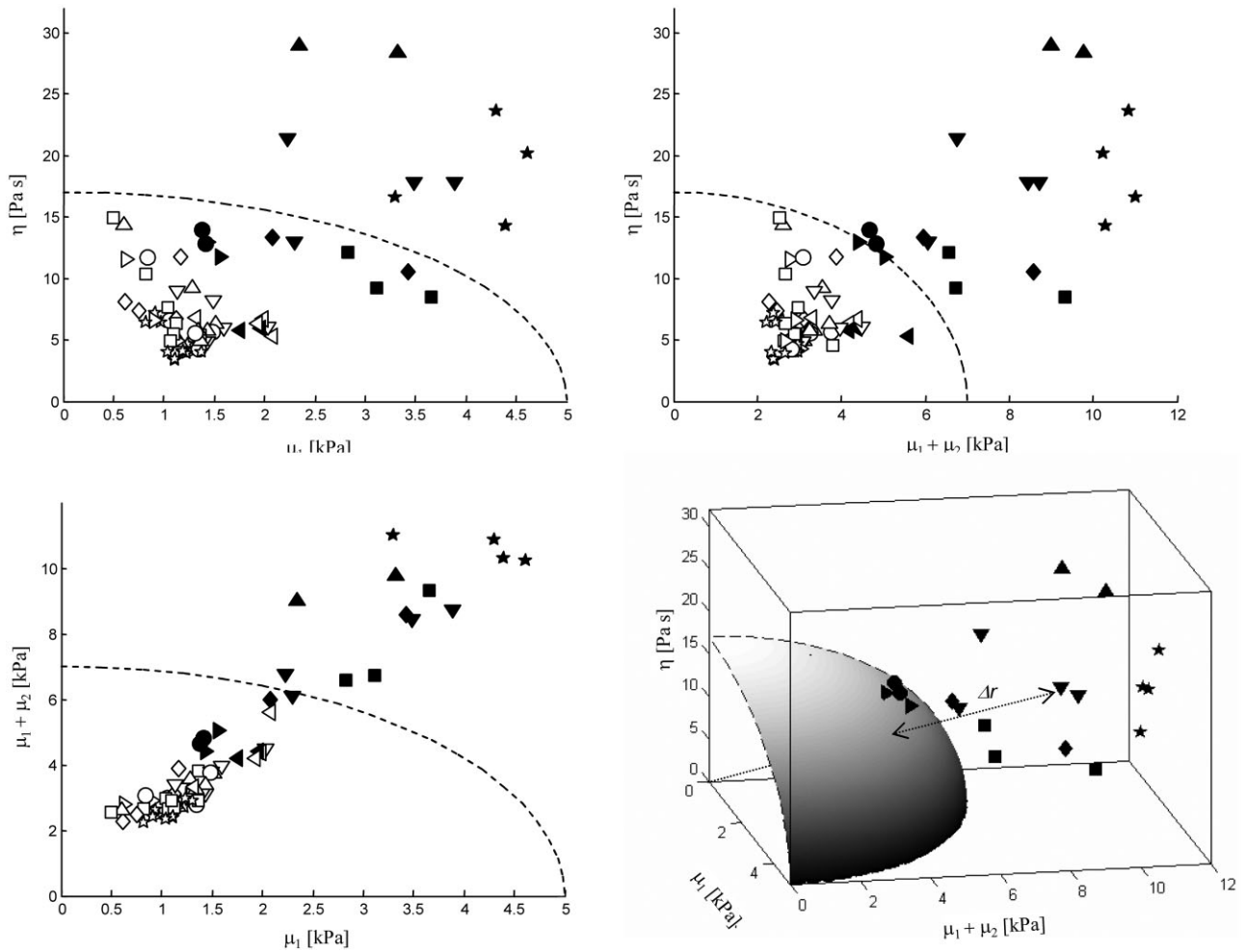


FIG. 6. Plot of all study results in the 3D parameter space given by μ_1 (static modulus), $\mu_1 + \mu_2$ (high frequency modulus), and η (viscosity). Open symbols correspond to healthy subjects; closed symbols indicate cirrhosis (each individual is assigned to one symbol, as in Table 1). 2D graphs display projections of the 3D plot in the lower right corner. The dashed lines show 2D threshold for differentiating the subgroups of healthy and diseased livers. The ellipsoidal surface of the threshold enclosing all healthy volunteers and patient 3 is drawn in the 3D plot.

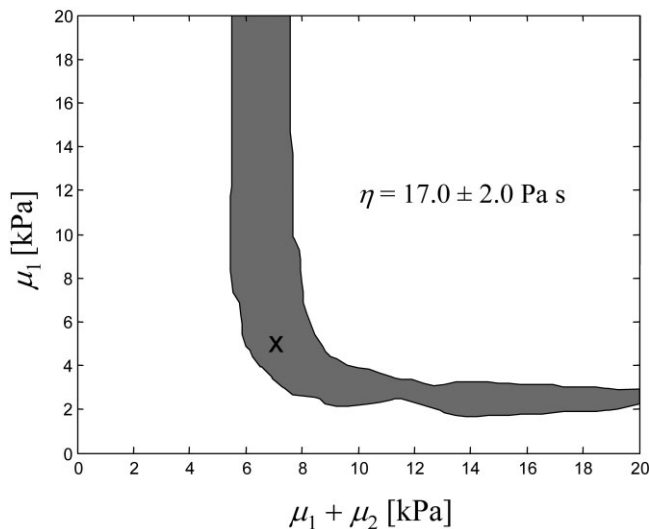


FIG. 7. Range of viscoelastic thresholds (gray patch and given η) that allows a differentiation of healthy and cirrhotic liver. The cross corresponds to the values used in Fig. 6.

normal liver and cirrhotic liver. The greater amount of information obtained from a multifrequency experiment allows the application of higher-order rheologic models for visualizing the dispersion of the respective tissue, as shown here. A more detailed mechanical characterization of organs potentially implies a more accurate detection of the disease process.

REFERENCES

- Dufour JF, DeLellis R, Kaplan MM. Reversibility of hepatic fibrosis in autoimmune hepatitis. *Ann Intern Med* 1997;127:981–985.
- Hammel P, Couvelard A, O'Toole D, Ratouis A, Sauvanet A, Flejou JF, Degott C, Belghiti J, Bernades P, Valla D, Ruszniewski P, Levy P. Regression of liver fibrosis after biliary drainage in patients with chronic pancreatitis and stenosis of the common bile duct. *N Engl J Med* 2001;344:418–423.
- Friedman SL. Liver fibrosis—from bench to bedside. *J Hepatol* 2003;38(Suppl 1):S38–S53.
- Parker KJ, Huang SR, Musulin RA, Lerner RM. Tissue response to mechanical vibrations for “sonoelasticity imaging”. *Ultrasound Med Biol* 1990;16:241–246.
- Ophir J, Céspedes I, Ponnekanti H, Yazdi Y, Li X. Elastography: a quantitative method for imaging the elasticity of biological tissues. *Ultrasound Imaging* 1991;13:111–134.
- Muthupillai R, Lomas DJ, Rossman PJ, Greenleaf JF, Manduca A, Ehman RL. Magnetic resonance elastography by direct visualization of propagating acoustic strain waves. *Science* 1995;269:1854–1857.
- Plewes DB, Betty I, Urchuk SN, Soutar I. Visualizing tissue compliance with MR imaging. *J Magn Reson Imaging* 1995;5:733–738.
- Sandrin L, Fourquet B, Hasquenoph JM, Yon S, Fournier C, Mal F, Christidis C, Ziol M, Poulet B, Kazemi F, Beaugrand M, Palau R. Transient elastography: a new noninvasive method for assessment of hepatic fibrosis. *Ultrasound Med Biol* 2003;29:1705–1713.
- Ziol M, Handra-Luca A, Kettaneh A, Christidis C, Mal F, Kazemi F, de Ledinghen V, Marcellin P, Dhumeaux D, Trinchet JC, Beaugrand M. Noninvasive assessment of liver fibrosis by measurement of stiffness in patients with chronic hepatitis C. *Hepatology* 2005;41:48–54.
- Rouviere O, Yin M, Dresner MA, Rossman PJ, Burgart LJ, Fidler JL, Ehman RL. MR elastography of the liver: preliminary results. *Radiology* 2006;240:440–448.
- Huwart L, Peeters F, Sinkus R, Annet L, Salameh N, ter Beek LC, Horsmans Y, Van Beers BE. Liver fibrosis: non-invasive assessment with MR elastography. *NMR Biomed* 2006;19:173–179.
- Klatt D, Asbach P, Rump J, Papazoglou S, Somasundaram R, Modrow J, Braun J, Sack I. In vivo determination of hepatic stiffness using steady-state free precession magnetic resonance elastography. *Invest Radiol* 2006;41:841–848.
- Yin M, Woollard J, Wang X, Torres VE, Harris PC, Ward CJ, Glaser KJ, Manduca A, Ehman RL. Quantitative assessment of hepatic fibrosis in an animal model with magnetic resonance elastography. *Magn Reson Med* 2007;58:346–353.
- Kruse SA, Smith JA, Lawrence AJ, Dresner MA, Manduca A, Greenleaf JF, Ehman RL. Tissue characterization using magnetic resonance elastography: preliminary results. *Phys Med Biol* 2000;45:1579–1590.
- Klatt D, Hamhaber U, Asbach P, Braun J, Sack I. Noninvasive assessment of the rheological behavior of human internal organs using multifrequency MR elastography: a study of brain and liver viscoelasticity. *Phys Med Biol* 2007;52:7281–7294.
- Sack I, Beierbach B, Hamhaber U, Klatt D, Braun J. Non-invasive measurement of brain viscoelasticity using magnetic resonance elastography. *NMR Biomed* 2008;21:265–271.
- Sinkus R, Siegmann K, Xydeas T, Tanter M, Claussen C, Fink M. MR elastography of breast lesions: Understanding the solid/liquid duality can improve the specificity of contrast-enhanced MR mammography. *Magn Reson Med* 2007;58:1135–1144.
- Manduca A, Lake DS, Kugel JL, Rossman PJ, Ehman RL. Dispersion measurements from simultaneous multi-frequency MR elastography. In: *Proceedings of the 11th Annual Meeting of ISMRM, Toronto, Ontario, Canada, 2003 (Abstract 550)*.
- Muthupillai R, Ehman RL. Spectrally-selective gradient waveforms: applications in MR elastography. In: *Proceedings of the 6th Annual Meeting of ISMRM, Sydney, Australia, 1998 (Abstract 2180)*.
- Rump J, Klatt D, Braun J, Warmuth C, Sack I. Fractional encoding of harmonic motions in MR elastography. *Magn Reson Med* 2007;57:388–395.
- Tschoegl NW. *The phenomenological theory of linear viscoelastic behavior*. Berlin: Springer; 1989.
- Liu Z, Bilston L. On the viscoelastic character of liver tissue: experiments and modelling of the linear behaviour. *Biorheology* 2000;37:191–201.
- Kiss MZ, Varghese T, Hall TJ. Viscoelastic characterization of in vitro canine tissue. *Phys Med Biol* 2004;49:4207–4218.
- Valtorta D, Mazza E. Measurement of rheological properties of soft biological tissue with a novel torsional resonator device. *Rheologica Acta* 2006;45:677–692.
- Yin M, Talwalkar JA, Grimm RC, Rossman PJ, Manduca A, Ehman RL. Diagnosis of hepatic fibrosis by magnetic resonance elastography: sensitivity and specificity. In: *Proceedings of the 15th Annual Meeting of ISMRM, Berlin, Germany, 2007 (Abstract 214)*.